Experimental demonstration of metamaterial anisotropy engineering for broadband on-chip polarization beam splitting

ALAINE HERRERO-BERMELLO,[1,5,*] ◉ ANTONIO DIAS-PONTE,[2] JOSÉ MANUEL LUQUE-GONZÁLEZ,[3] ◉ ALEJANDRO ORTEGA-MOÑUX,[3] AITOR V. VELASCO,[1] PAVEL CHEBEN,[4] ◉ AND ROBERT HALIR[3]

[1]*Instituto de Óptica, Consejo Superior de Investigaciones Científicas, Madrid 28006, Spain*
[2]*Alcyon Photonics S.L., Madrid 28006, Spain*
[3]*Universidad de Málaga, Depto. De Ingeniería de Comunicaciones, ETSI de Telecomunicación, Campus de Teatinos s/n, Málaga 29071, Spain*
[4]*National Research Council of Canada, Ottawa, Ontario K1A 0R6, Canada*
[5]*Currently with Alcyon Photonics S.L. Madrid, Spain*
*alaine.herrero@csic.es

Abstract: Subwavelength metamaterials exhibit a strong anisotropy that can be leveraged to implement high-performance polarization handling devices in silicon-on-insulator. Whereas these devices benefit from single-etch step fabrication, many of them require small feature sizes or specialized cladding materials. The anisotropic response of subwavelength metamaterials can be further engineered by tilting its constituent elements away from the optical axis, providing an additional degree of freedom in the design. In this work, we demonstrate this feature through the design, fabrication and experimental characterization of a robust multimode interference polarization beam splitter based on tilted subwavelength gratings. A 110-nm minimum feature size and a standard silicon dioxide cladding are maintained. The resulting device exhibits insertion loss as low as 1 dB, an extinction ratio better than 13 dB in a 120-nm bandwidth, and robust tolerances to fabrication deviations.

1. Introduction

Subwavelength gratings (SWGs) are periodic arrangements of alternating materials with a pitch smaller than the wavelength of light propagating through them [1]. Since diffraction is frustrated under these conditions, a SWG behaves as a metamaterial with a refractive index and dispersive properties that can be lithographically engineered [2]. In silicon photonics, the availability of high-resolution lithography techniques has enabled the use of SWGs in a wide array of applications, ranging from high-performance fiber-to-chip couplers [3,4], to enhanced photonic biosensors [5–7], advanced filters [8,9] and mid-infrared waveguide platforms [10]. The metamaterial synthesized by a SWG is strongly anisotropic, because the electric field experiences different boundary condition depending on whether the subwavelength segments are oriented parallel or perpendicular to the direction of propagation [2]. This property has been exploited to demonstrate broadband beam-splitters [11] and to minimize coupling between adjacent waveguides [12], but also finds direct application in on-chip polarization handling.

Polarization beam splitters and polarization rotators are key components for silicon photonics chips, as they enable polarization diversity circuits that address the strong polarization dependence of silicon waveguides [13]. High-performance polarization beam splitters can be implemented using a variety of approaches including directional couplers [14,15], bi-level tapered waveguides [16,17], and partially etched multimode interference couplers (MMIs) [18]. These complex fabrication requirements can be circumvented by exploiting the anisotropic properties of SWGs,

hence enabling the design of single etch polarization beam splitters for a variety of silicon thicknesses with remarkable performance [19–21]. While SWG-based splitters with extinction ratios (ER) in excess of 20 dBs, insertion losses (IL) well below 1 dB and bandwidths in excess of 150 nm have been reported, they often exhibit sub-100-nm minimum feature sizes (MFS) and use specialized cladding materials, such as SU-8, to achieve a good filling of the small gaps between the subwavelength elements [21]. However, for many silicon opto-electronics platforms, feature sizes of at least 100 nm are required and silicon dioxide is preferred as a cladding material [22–24].

Recently, we proposed tilted gratings as a novel approach for engineering the anisotropic properties of SWG metamaterials [25]. Tilting each individual segment of a SWG waveguide away from the transverse direction significantly modifies TE effective refractive index, whereas TM mode remains almost unaffected. This principle was leveraged in the theoretical design of an MMI polarization beam splitter [26], resulting in a compact device under 100 μm long. Tilted SWGs were also applied to a polarization-independent monomode waveguide [27], achieving a birefringence under 6.10^{-3} in a 100-nm bandwidth around a central wavelength of 1550 nm. However, both devices had, so far, only been proposed theoretically.

Building on our theoretical work in [26], here we experimentally demonstrate, for the first time, material anisotropy engineering with tilted subwavelength segments in a polarization beam splitter. We furthermore show that the additional degree of freedom gained from tilting the elements enables feature sizes larger than 100 nm and can compensate incomplete filling of the subwavelength gaps with the silicon dioxide cladding. Our device exhibits IL below 1 dB and an ER better than 13 dB in a 120-nm bandwidth, thus exceeding the requirements for optical communications in the full C and L bands [28].

2. Design

Our device, illustrated in Fig. 1, is based on an MMI composed of tilted subwavelength segments. When the fundamental modes with TE (horizontal) and TM (vertical) polarization are launched into input 1, the self-image of the TE polarized mode is formed at output 2, while the TM polarized mode is imaged at output 3. This requires a specific relation between the beat lengths of both polarizations, L_π^{TM} and L_π^{TE}: $(2m - 1)L_\pi^{TM} = 2nL_\pi^{TE}$, where m and n are integers [29]. Tilting the SWG segments an angle θ with respect to the transversal direction (x) enables us to modify the anisotropy of the resulting equivalent medium [25], thereby achieving the required relation between L_π^{TM} and L_π^{TE} even with $m = n = 1$ (that is, $L_\pi^{TM} = 2L_\pi^{TE}$), which is the shortest possible configuration. To ensure a smooth transition between the interconnecting waveguides and the tilted SWG region, and hence minimize back reflection (BR), the SWG segments of the input and output tapers are rotated progressively as illustrated in Fig. 1(a). Additionally, these tapers also widen the input waveguides to control the number of modes that are excited in the multimode region. By means of 3D-FDTD simulations in a back to back configuration, we estimate a transition taper length of $L_t = 13$ μm (50 periods) for a transition with negligible loss and back reflections between the homogeneous and periodic structures. Then, the taper final width (W_t) is tuned to optimize MMI mode excitation, hence minimizing IL and BR of the full device. An optimum value of $W_t = 1.5$ μm is obtained.

The duty-cycle of the SWG structure is kept constant along the whole device, with a value of 50% to maximize MFS and facilitate fabrication. The SWG period is optimized to $\Lambda = 220$ nm to maximize the bandwidth of the device, resulting in an MFS of $a = b = 110$ nm for both the silicon segments and the gaps [see Fig. 1(a)]. In our previous work in [26], we assumed a complete filling of the gaps with the silicon dioxide cladding. The beat lengths for both polarizations were calculated from the effective indices of the Bloch modes of the segmented structure for different tilt angles. Bloch modes were calculated using the procedure described in [30]. The results showed that the tilt angle that yields the desired relation between L_π^{TM} and
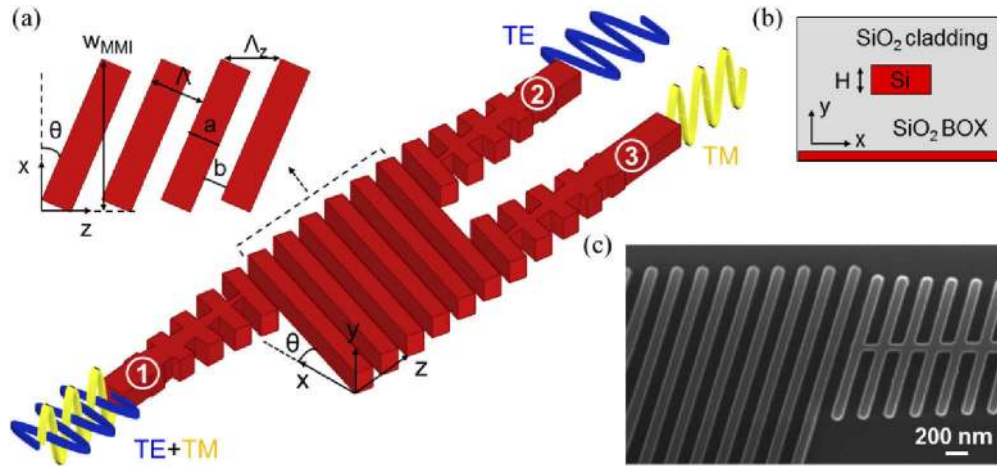
Fig. 1. (a) Schematic of the multimode interference coupler-based polarization beam splitter and a top view of the multimode region (inset); (b) layer structure of the device; and (c) scanning electron microscope image of output port 2 of the polarization beam splitter for a tilt angle of 15°. The image was taken prior to the deposition of the SiO$_2$ cladding.

L_π^{TE} was between 7° and 9°for a wavelength of 1.55 µm and a 220-nm-thick silicon layer (H). Further optimizations through iterative 3D-FDTD simulations resulted in an optimized design with a tilt angle of 7° and a length of 92.4 µm comprising 417 periods [26]. The remaining dimensions of the device are summarized in Table 1. As illustrated in Fig. 2(a) the device achieves a simulated bandwidth of 130 nm for IL below 1 dB and ER better than 20 dB. Here, IL and ER are defined as $IL^{TE} = 10 \log(P_1^{TE}/P_2^{TE})$, $IL^{TM} = 10 \log(P_1^{TM}/P_3^{TM})$, $ER^{TE} = 10 \log(P_2^{TE}/P_3^{TE})$, $ER^{TM} = 10 \log(P_3^{TM}/P_2^{TM})$, where P_i^{TE} and P_i^{TM} are the power in the fundamental TE and TM polarized modes in waveguide i [see Fig. 1(a)]. The simulations are carried out with a commercial 3D-FDTD software [31], using a carefully optimized grid of 17 nm and 11 nm in the y and z directions, respectively, to ensure that the tilted segments are properly sampled. Owing to the relatively large width of the device, a more relaxed and angle dependent grid equal to $grid_z/tan(\theta)$ can be used in the x direction. The simulation window is 5.6 µm wide in the x direction and 2.8 µm high in the y direction.

Table 1. Optimized parameters of the MMI-based PBS when the cladding fully penetrates the gaps between the silicon segments and when a thin air layer is present.

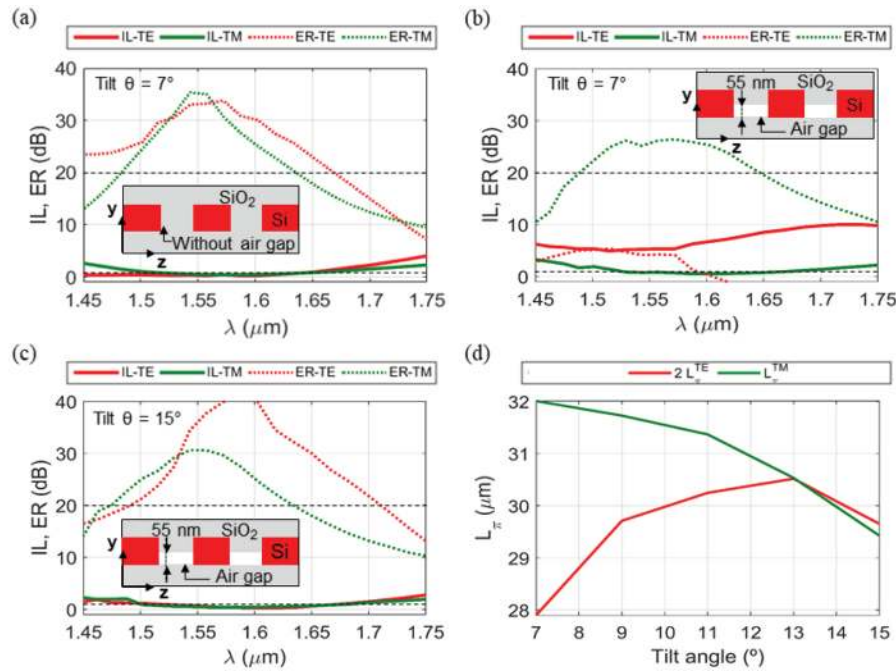| Parameter	Gaps fully-filled with SiO$_2$	Gaps with SiO$_2$ and a 55-nm air layer
Silicon thickness (H)	220 nm	
Tilt angle (θ)	7 °	15 °
MMI length (L_{MMI})	92.4 µm	91.1 µm
Number of periods (N)	417	400
Period (Λ)	220 nm	
Duty cycle (DC)	50%	
MMI width (W_{MMI})	4 µm	
Transition taper final width (W_t)	1.5 µm	
Transition taper length (L_t)	13 µm	
Transition taper number of periods (N_t)	50	

Fig. 2. (a) Simulated insertion losses (IL) and extinction ratio (ER) of the polarization beam splitter with a 7° tilt and without considering any air gap between the silicon segments. (b) The inclusion of small air gaps results in a significant detuning of the device. (c) Device performance can be restored by increasing the tilt angle to 15° tilt PBS. Dashed black lines mark ER greater than 20 dB and IL below 1 dB. (d) Simulated beat lengths of TE and TM modes for different tilt angles for an air gap depth of 55 nm.

However, this initial nominal design does not take into account incomplete filling of the gaps with the silicon dioxide cladding, often observed in SWG structures [11]. This phenomenon results in small air holes under the cladding sections, as illustrated in the inset of Fig. 2(b). These holes will affect the TE and TM polarizations differently, breaking the desired relation between the beat lengths (i.e. $L_\pi^{TM} \neq 2L_\pi^{TE}$) and thus degrading device performance. In order to determine the specific air gap depth present in our device, we considered an initial estimation of 60 nm based on the findings of [11]. This parameter was incorporated into our FDTD simulation and further refined by comparing simulation results with the experimental characterization of the MMI nominal design (i.e. $\theta = 7°$) while slightly varying said initial estimation, achieving the best fit for a 55-nm air gap. Note that the effect of these air gaps depends mainly on the area of their cross section and not on their specific shape [11], so rectangular holes were considered during the simulation process. The situation is analyzed in Fig. 2(b), where a 55-nm air gap has been included in the simulations, leaving all other device parameters unchanged. We observe that the beat length for TM polarization is not strongly affected: the device maintains an ER above 20 dB in the full 130-nm bandwidth, while IL are kept below 1.6 dB. This is expected since the TM modes are only weakly confined in the vertical direction and thus are not strongly affected by the air gap. Conversely, this perturbation has a stronger effect for TE polarization, resulting in a significant reduction of the beat length and detuning the device. Since for TE polarization SWG-based MMIs are furthermore almost wavelength independent [11], the device remains detuned in the full 130-nm wavelength range, as shown in Fig. 2(b). Note that while the device could be retuned for TE polarization by shortening its length, this would result in a detuning for

TM polarization. Other approach to mitigate the oxide filling problem would be to increase the period of the SWG structure, although this would entail reducing device bandwidth as the SWG metamaterial gets closer to the Bragg regime.

In this work, we propose to solve this problem of incomplete cladding filling by adjusting the tilt angle of the SWG segments, readily compensating the effect of the air holes. Indeed, while the air gaps result in a reduction of beat length for TE polarization, increasing the tilt angle reverses this effect. Critically, it does so while maintaining the 50% duty-cycle and the large MFS of 110 nm. In order to determine the updated value of the tilt angle, the 55-nm air holes were incorporated to the theoretical model, and the device was reoptimized following the process disclosed in [26]. That is, beat lengths for both polarizations were calculated from the effective indices of the Bloch modes of the segmented structure for different tilt angles. As show in Fig. 2(d), the device can be re-tuned for an approximate tilt angle of 13°. Further optimization through 3D – FDTD simulations leads to an optimum tilt angle of $\theta = 15°$ for verifying the necessary relation between the beat lengths of both polarizations ($L_\pi^{TM} = 2L_\pi^{TE}$). The optimum number of periods changes slightly to 400, but all other geometrical parameters remain unchanged, as shown in Table 1. The simulated performance of the device with a $\theta = 15°$ tilt angle and 55-nm air holes is depicted in Fig. 2(c), showing an ER in excess of 20 dB and IL below 1 dB in the full 130-nm bandwidth. Negligible BR under -53 dB is also achieved within the whole bandwidth.

3. Fabrication and experimental results

To experimentally evaluate the performance of the polarization splitter and the anisotropy engineering properties of tilted SWG waveguides, a series of devices with different tilt angles were fabricated. Silicon-on-insulator (SOI) wafers with standard 220-nm-thick silicon on top of a 2-μm buried oxide (BOX) were used [see Fig. 1(b)]. Waveguides were defined in a single patterning step by electron beam lithography, and inductively coupled plasma reactive ion etching was used to transfer the resist pattern into the silicon layer. A 3-μm silicon dioxide upper cladding was deposited using a chemical vapor deposition (CVD) process. Note that even with a 1-μm-thick cladding layer, the leakage losses of the weakly confined TM polarization are below 0.1 dB [26]. Figure 1(c) shows a scanning electron micrograph of the fabricated structure prior to the deposition of the SiO$_2$ cladding.

For experimental characterization, a tunable laser operating in the wavelength range from 1.495 μm to 1.64 μm was used. The laser was connected to an in-line polarizer (to increase the polarization extinction ratio), a polarization controller and a lensed fiber. Efficient sub-wavelength grating edge couplers were used for fiber-to-chip coupling [4], which at the same time reduces back-reflections thereby minimizing Fabry-Perot cavity effects. Output light was collected and collimated with a ×40 microscope objective and directed through a Glan-Thomson polarizer to obtain a single polarization state before detecting the optical power with a photodiode. Measurements were performed as follows: first, light was collected directly from the fiber tip, using the input polarization controller and the polarizer at the output to align the polarization to the horizontal or vertical state. In this configuration, we measured an ER between the horizontal and vertical states in excess of 20 dB in the full bandwidth of the laser. The devices were then measured for horizontal and vertical polarization. The ER was computed directly from the measurements of each device, while the IL were obtained by normalizing to the transmission of a reference waveguide for TE and TM polarization.

Our measurements confirm the presence of air holes in the cladding because, as predicted in our simulation, the device with a 7° tilt angle exhibits a poor performance for TE polarization, while an ER in excess of 20 dB is obtained for TM polarization. However, in accordance with our simulations, increasing the tilt angle of the subwavelength segments compensates the effect of the air holes, retuning the device. As shown in Fig. 3(a), the device exhibits IL below 1 dB for

both polarizations in the 1520 nm to 1640 nm band, hence exceeding the C and L bands. An ER well above 13 dB is obtained in this wavelength range. Both conditions are expected to continue above 1640 nm, but our experimental setup was limited by the laser source tuneability range. It should be noted that for applications in optical communications, an ER of this order entails only minimal penalties, because they are readily compensated in digital signal processing [28]. In this sense, IL are more critical, because they irremediably deteriorate the signal to noise ratio. Finally, by further incorporating a circulator in the experimental setup, experimental BR were determined to be under -30 dB, being this value limited by our measurement setup. Considering our setup limitation, as well as an expected slight ER degradation between simulation and experimental characterization, these results are in good agreement with the theoretical performance previously reported in [26], which presented a bandwidth of 128 nm (IL < 1dB, ER > 20dB).
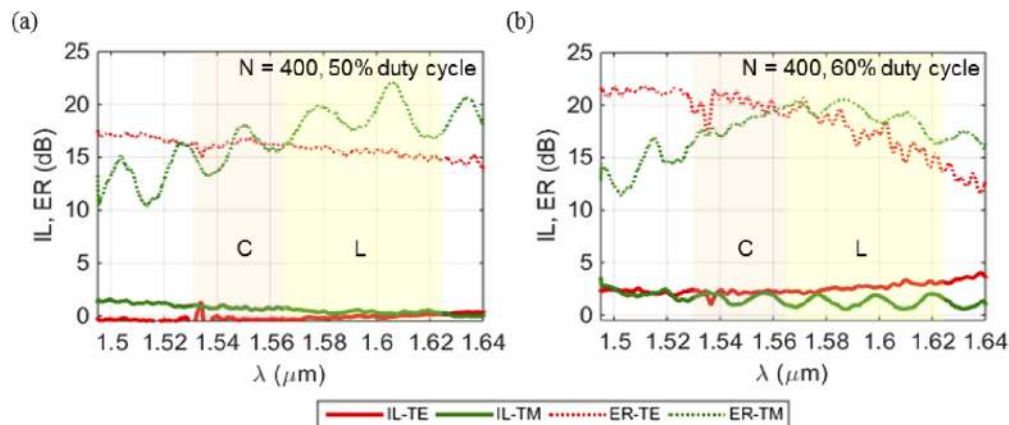

Fig. 3. Measured insertion loss (IL) and polarization extinction ratio (ER) for a device with a 15° tilt angle, 400 periods and a duty cycle of (a) 50% and (b) 60%. The geometrical parameters are summarized

Previous theoretical analysis showed a good resilience of the device to fabrication deviations [26], with a variation of $\pm 5\%$ in the duty cycle (i.e. ± 11 nm deviation in the length of the segments), leading to a just 1.5% reduction in the bandwidth of the device, maintaining ER > 20 dB and IL < 1 dB. In order to experimentally validate this behavior, we fabricated and characterized a design with a duty-cycle increase of 10% (i.e. silicon segments of 132 nm instead of 110 nm). Although this change has virtually no impact on the ER, it does increase IL to about 2 dB for TM polarization and 2.5 dB for TE polarization [Fig. 3(b)]. Moreover, in order to study tolerances against silicon layer thickness variations, 3D-FDTD simulations of the entire device are performed, for which the grid is reduced to 10 nm in y direction. Even for thickness variations of ± 10 nm, well over current tolerances of photonic manufacturing processes, the device preserves a good performance, with ER greater than 20 dB and IL better than 1 dB in a bandwidth of 129 nm for TE polarization and 118 nm for the TM polarization.

In cases where a greater fabrication robustness is required, this problem can be solved by modifying the number of periods of the MMI. We experimentally analyzed the robustness against the aforementioned DC variation of different versions of the MMI with a modified number of periods ranging from 380 to 430. Among these devices, the best robustness was achieved for 395 periods, as shown in Fig. 4. In Fig. 4(a) we show the experimental performance of a slightly shorter device, with 395 periods instead of the nominal value (400 periods). We observe that for TE polarization, the IL remain negligible, and that the ER increases slightly. The device becomes slightly detuned for TM polarization, however, since it retains ER better than 13 dB and IL increases with marginally higher IL of to 1.5 dB, but in a narrower bandwidth of 100 nm

(Fig. 4(a)). Nevertheless, a greater resilience to DC variations is achieved, with a 22-nm increase in the length of silicon segments having virtually no effect on the IL, and further improving the ER (Fig. 4(b)).
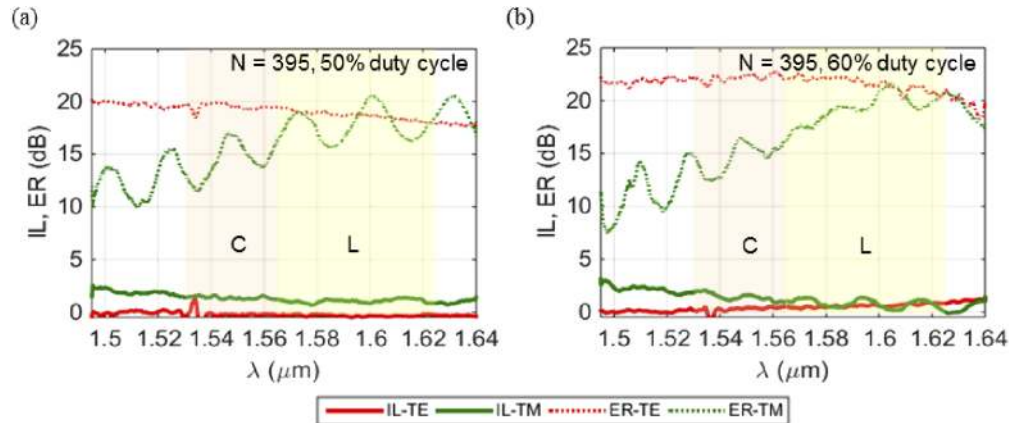

Fig. 4. Measured insertion loss (IL) and polarization extinction ratio (ER) for a device with a 15° tilt angle, 395 periods and a duty-cycle of (a) 50% and (b) 60%. The geometrical parameters are summarized in Table 1.

4. Conclusions

In summary, we have experimentally demonstrated the ability to tune material anisotropy through tilted subwavelength gratings in a broadband polarization beam splitter. This results in a device with large minimum feature sizes (110 nm) that can be readily integrated in opto-electronic CMOS platforms. Our device exhibits insertion losses below 1 dB and an extinction ratio better than 13 dB in a 120-nm bandwidth, thus exceeding the requirements for optical communications in the full C and L bands. The tilt angle of the subwavelength grating serves as an additional degree of freedom that can be used to compensate the effect of voids resulting from incomplete cladding filling. At the same time, fine tuning of the device length enables balancing performance and fabrication tolerances. We believe that our approach will pave the way towards broadband polarization splitters in silicon-photonics that can be readily incorporated into commercial opto-electronic platforms.

Funding

Disclosures

AHB: Alcyon Photonics S.L. (F,P), ADP: Alcyon Photonics S.L. (E,I), JMLG: Alcyon Photonics S.L. (F), AOM: Alcyon Photonics S.L. (F,P), AVV: Alcyon Photonics S.L. (F,I,P), RH: Alcyon Photonics S.L. (F,P).

References

1. R. Halir, A. Ortega-Moñux, D. Benedikovic, G. Z. Mashanovich, J. G. Wangüemert-Pérez, J. H. Schmid, I. Molina-Fernández, and P. Cheben, "Subwavelength-grating metamaterial structures for silicon photonic devices," Proc. IEEE **106**(12), 2144–2157 (2018).
2. P. Cheben, R. Halir, J. Schmid, H. Atwater, and D. Smith, "Subwavelength integrated photonics," Nature **560**(7720), 565–572 (2018).
3. P. Cheben, D. -X. Xu, S. Janz, and A. Densmore, "Subwavelength waveguide grating for mode conversion and light coupling in integrated optics," Opt. Express **14**(11), 4695–4702 (2006).
4. P. Cheben, J. H. Schmid, S. Wang, D.-X. Xu, M. Vachon, S. Janz, J. Lapointe, Y. Painchaud, and M.-J. Picard, "Broadband polarization independent nanophotonic coupler for silicon waveguides with ultra-high efficiency," Opt. Express **23**(17), 22553–22563 (2015).
5. J. G. Wangüemert-Pérez, A. Hadij-ElHouati, A. Sánchez-Postigo, J. Leuermann, D.-X. Xu, P. Cheben, A. Ortega-Moñux, R. Halir, and I. Molina-Fernández, "Subwavelength structures for silicon photonics biosensing," Opt. Laser Technol. **109**, 437–448 (2019).
6. E. Luan, H. Yun, M. Ma, D. M. Ratner, K. C. Cheung, and L. Chrostowski, "Label-free biosensing with a multi-box sub-wavelength phase-shifted Bragg grating waveguide," Biomed. Opt. Express **10**(9), 4825–4838 (2019).
7. L. Torrijos-Morán, A. Griol, and J. García-Rupérez, "Experimental study of subwavelength grating bimodal waveguides as ultrasensitive interferometric sensors," Opt. Lett. **44**(19), 4702–4705 (2019).
8. P. Cheben, J. Ctyroký, J. H. Schmid, S. Wang, J. Lapointe, J. G. Wangüemert-Pérez, I. Molina-Fernández, A. Ortega-Moñux, R. Halir, D. Melati, D. Xu, S. Janz, and M. Dado, "Bragg filter bandwidth engineering in subwavelength grating metamaterial waveguides," Opt. Lett. **44**(4), 1043–1046 (2019).
9. H. Yun, M. Hammood, S. Lin, L. Chrostowski, and N. A. F. Jaeger, "Broadband flat-top SOI add–drop filters using apodized sub-wavelength grating contradirectional couplers," Opt. Lett. **44**(20), 4929–4932 (2019).
10. J. S. Penadés, A. Sánchez-Postigo, M. Nedeljkovic, A. Ortega-Moñux, J. G. Wangüemert-Pérez, Y. Xu, R. Halir, Z. Qu, A. Z. Khokhar, A. Osman, W. Cao, C. G. Littlejohns, P. Cheben, I. Molina-Fernández, and G. Z. Mashanovich, "Suspended silicon waveguides for long-wave infrared wavelengths," Opt. Lett. **43**(4), 795–798 (2018).
11. R. Halir, P. Cheben, J. M. Luque-González, J. D. Sarmiento-Merenguel, J. H. Schmid, G. Wangüemert-Perez, D. X. Xu, S. Wang, A. Ortega-Moñux, and I. Molina-Fernández, "Ultrabroadband nanophotonic beamsplitter using an anisotropic SWG material," Laser Photonics Rev. **10**(6), 1039–1046 (2016).
12. S. Jahani, S. Kim, J. Atkinson, J. C. Wirth, F. Kalhor, A. A. Noman, W. D. Newman, P. Shekhar, K. Han, V. Van, R. G. DeCorby, L. Chrostowski, M. Qi, and Z. Jacob, "Controlling evanescent waves using silicon photonic all-dielectric metamaterials for dense integration," Nat. Commun. **9**(1), 1893 (2018).
13. D. Dai, L. Liu, S. Gao, D.-X. Xu, and S. He, "Polarization management for silicon photonic integrated circuits," Laser Photonics Rev. **7**(3), 303–328 (2013).
14. H. Wu, Y. Tan, and D. Dai, "Ultra-broadband high-performance polarizing beam splitter on silicon," Opt. Express **25**(6), 6069–6075 (2017).
15. C. Li and D. Dai, "Compact polarization beam splitter based on a three-waveguide asymmetric coupler with a 340-nm-thick silicon core layer," J. Lightwave Technol. **36**(11), 2129–2134 (2018).
16. Y. Tian, J. Qiu, C. Liu, S. Tian, Z. Huang, and J. Wu, "Compact polarization beam splitter with a high extinction ratio over S + C+L band," Opt. Express **27**(2), 999–1009 (2019).
17. T. Barwicz, M. R. Watts, M. A. Popovic, P. T. Rakich, L. Socci, F. X. Kärtner, E. P. Ippen, and H. I. Smith, "Polarization-transparent microphotonic devices in the strong confinement limit," Nat. Photonics **1**(1), 57–60 (2007).
18. X. Sun, J. S. Aitchison, and M. Mojahedi, "Realization of an ultra-compact polarization beam splitter using asymmetric MMI based on silicon nitride / silicon-on-insulator platform," Opt. Express **25**(7), 8296–8305 (2017).
19. L. Liu, Q- Deng, and Z. Zhou, "Manipulation of the beat length and wavelength dependence of a polarization beam splitter using a subwavelength grating," Opt. Lett. **41**(21), 5126–5129 (2016).
20. L. Xu, Y. Wang, A. Kumar, D. Patel, E. El-Fiky, Z. Xing, R. Li, and D. V. Plant, "Polarization beam splitter based on MMI coupler with SWG Birefringence engineering on SOI," IEEE Photon. Technol. Lett. **30**(4), 403–406 (2018).
21. H. Xu, D. Dai, and Y. Shi, "Ultra-broadband and ultra-compact on-chip silicon polarization beam splitter by using hetero-anisotropic metamaterials," Laser Photonics Rev. **13**(4), 1800349 (2019).
22. M. Pantouvaki, S. A. Srinivasan, Y. Ban, P. De Heyn, P. Verheyen, G. Lepage, H. Chen, J. De Coster, N. Golshani, S. Balakrishnan, P. Absil, and J. V. Campenhout, "Active components for 50Gb/s NRZ-OOK optical interconnects in a silicon photonics platform," J. Lightwave Technol. **35**(4), 631–638 (2017).
23. B. Szelag, K. Hassan, L. Adelmini, E. Ghegin, P. Rodríguez, F. Nemouchi, P. Brianceau, E. Vermande, A. Schembri, D. Carrara, P. Cavalié, F. Franchin, M.-C. Roure, L. Sánchez, C. Jany, and S. Olivier, "Hybrid III-V/silicon technology for laser integration on a 200-mm fully CMOS-compatible silicon photonics platform," J.Sel. Top. Quantum Eletron. **25**(5), 1–10 (2019).
24. M. Ma, A. H. K. Park, Y. Wang, H. Shoman, F. Zhang, N. A. F. Jaeger, and L. Chrostowski, "Sub-wavelength grating-assisted polarization splitter-rotators for silicon-on-insulator platforms," Opt. Express **27**(13), 17581–17591 (2019).
25. J. M. Luque-González, A. Herrero-Bermello, A. Ortega-Moñux, I. Molina-Fernández, A. V. Velasco, P. Cheben, J. H. Schimd, S. Wang, and R. Halir, "Tilted subwavelength gratings: controlling anisotropy in a metamaterial," Opt. Lett. **43**(19), 4691–4694 (2018).

26. A. Herrero-Bermello, J. M. Luque-González, A. V. Velasco, A. Ortega-Moñux, P. Cheben, and R. Halir, "Design of a broadband polarization splitter based on anisotropy-engineered tilted subwavelength gratings," IEEE Photonics J. **11**(3), 1–8 (2019).

27. A. Herrero-Bermello, J. M. Luque-González, R. Halir, P. Cheben, A. Ortega-Moñux, I. Molina-Fernández, and A. V. Velasco, "Zero-birefringence silicon waveguides based on tilted subwavelength metamaterials," IEEE Photonics J. **11**(5), 1–8 (2019).

28. P. J. Reyes-Iglesias, I. Molina-Fernández, and A. Ortega-Moñux, "Sensitivity penalty induced by non-ideal dual polarization downconverter in digital coherent receivers," Opt. Express **23**(10), 12784–12794 (2015).

29. M. Yin, W. Yang, Y. Li, X. Wang, and H. Li, "CMOS-compatible and fabrication-tolerant MMI-based polarization beam splitter," Opt. Commun. **335**, 48–52 (2015).

30. J. G. Wangüemert-Pérez, P. Cheben, A. Ortega-Moñux, C. Alonso-Ramos, D. Pérez-Galacho, R. Halir, I. Molina-Fernández, D.-X. Xu, and J. H. Schmid, "Evanescent field waveguide sensing with subwavelength grating structures in silicon-on-insulator," Opt. Lett. **39**(15), 4442–4445 (2014).

31. 'FULLWAVE', Rsoft Products, Synopsys, 2019. Available: https://www.rsoftdesign.com.